

Analysis and Prediction of Anomalous Weather and Atmospheric Hazards

Hiromasa KAWAI, Tatsuya IWASHIMA, Hirohiko ISHIKAWA,
Takashi MARUYAMA, Hitoshi MUKOUGAWA,
Mitsuaki HORIGUCHI, Takao IGUCHI and Tokihiko ARAKI

Synopsis

This paper describes the analysis of anomalous weather and its hazards, which consists of three parts. The first part describes the predictability of a downward migration of the negative Northern Annular Mode (NAM) anomaly following a stratospheric sudden warming (SSW) occurring in January 2003. The second part describes strong wind disasters caused by typhoon, tornados and down bursts in 2006. The last part describes wind pattern of the descending high-speed turbulence structure in the nearly neutral atmospheric boundary layer and the possibility of tornado prediction with environmental parameter.

Keywords: anomalous weather, predictability, ensemble prediction, northern annular mode, stratospheric sudden warming, Typhoon 0613, strong wind, damage, turbulence structure, atmospheric boundary layer, tornado, EHI

1. Predictability of the Downward Migration of the Northern Annular Mode: A Case Study for January 200

1.1 Introduction

Recent studies have revealed that the understanding of the downward influence of the stratospheric circulation change on the troposphere is important to improve the forecast skill of the extended-range predictions. In particular, the Northern Annular Mode (NAM) corresponding to the dominant mode of the extratropical atmosphere is considered to be a key component to understand such downward influence of the stratosphere due to its downward migration characteristics revealed by Baldwin and Dunkerton (1999, 2001). The NAM is characterized by the variation in the strength of the zonal-mean zonal flow along 55°N, and related to the occurrence of the anomalous weather condition. Baldwin et al. (2003) proposed a statistical method to predict the monthly-mean Arctic Oscillation (AO) signature in the lower atmosphere using the preceding NAM index in the lower stratosphere. The AO signature is identical to

the NAM index at 1000 hPa. Since the variation of the predicted AO signature based on the preceding NAM index at 150 hPa is larger than that based on the preceding AO signature, they insisted the validity of the proposed statistical method to predict the AO signature. However, the practical limit of the predictability of the AO signature associated with the downward migration of the NAM has not been revealed using operational extended-range numerical prediction results.

On the other hand, our recent works [Mukougawa and Hirooka, 2004 (hereafter M04); Mukougawa et al., 2005 (hereafter M05)] indicated the prolonged predictability of stratospheric circulation during stratospheric sudden warming (SSW) events up to 1 month using the Japan Meteorological Agency (JMA) 1-month prediction results. The prolonged predictability is associated with the long time-scale inherent to the planetary waves propagating upward from the troposphere before the SSW events. Moreover, since the stratospheric circulation during the SSW events is characterized by negatively large NAM anomalies which descend gradually, we could expect prolonged predictability of negative AO events after

SSW episodes. Thus, in this study, we will examine the dynamics and the predictability of downward migration of negative NAM anomalies observed in January 2003 just after a SSW event using all members of the JMA 1-month ensemble prediction results. We will also try to reveal the precursory event for the downward migration of the negative NAM anomaly to the troposphere.

1.2 Data and Analysis Method

We used operational ensemble 1-month (34-day) forecast data sets provided by the JMA from November 2003 to January 2004. The JMA ensemble 1-month prediction has been carried out at 1200UTC every Wednesday and Thursday with 12 perturbed and 1 unperturbed initial conditions. Numerical integrations are conducted using a JMA global spectral model (JMA-GSM0103) with triangular 106 truncation (T106) and 40 vertical levels up to 0.4 hPa. For further model details, the reader should refer to M05. The initial perturbations are obtained using the Breeding of Growing Modes (BGM) method (Toth and Kalnay, 1993). The forecast data have been archived every 24 h for the 34-day prediction period on a 2.5-degree longitude-latitude grid at 22 levels from 1000 to 1 hPa. To verify model forecasts, JMA Global Analyses data set with 1.25-degree horizontal resolution at 23 levels from 1000 to 0.4 hPa is used.

As in M04, we also used the operational ECMWF twice-daily data set during 1985–2001 with 2.5-degree horizontal resolution at 14 levels from 1000 to 10 hPa to obtain the NAM index by the following procedure. First, the seasonal cycle, averaged over 17 years and subject to 5-day running average, is removed from the daily geopotential height on each gridpoint to define height anomalies. After applying a 10-day low-pass filter (Blackmon, 1976) to the anomalies, we perform a combined EOF analysis which combines geopotential height field at 50, 500, and 1000 hPa levels as in Yamazaki and Shinya (1999) to the low-pass filtered wintertime (November–April) anomalies. The analysis domain is poleward of 20N, and the grid data are weighted by the square root of the cosine of latitude as well as the square root of density at each level. The leading combined EOF mode corresponding to the NAM accounts for 11.3% of the total variance. Finally, the NAM index at each level is defined as the projection of the daily anomaly field onto the regression map

associated with the first EOF mode.

1.3 Results

During January 2003, a warming episode took place in the Northern Hemisphere stratosphere (Fig. 1), corresponding to a negatively large NAM event in the stratosphere. The SSW was caused by the amplification of zonal wavenumber (WN) 1 components. After the SSW, the negative NAM anomaly migrates downward to the surface from 17 through 21 January. In order to analyze the dynamics of the downward migration, the zonal-mean zonal wind acceleration averaged over 50N–70N is also shown in the bottom panel of Fig. 1. The deceleration at 10 hPa around 15 January is associated with the SSW due to the amplified WN 1 component. The deceleration extends down to the lower troposphere accompanied with the downward migration of the NAM index from 17 to 20 January. The gradual downward migration of the deceleration is confined within the stratosphere whereas the zonal wind concurrently decelerates over the entire troposphere around 18 January.

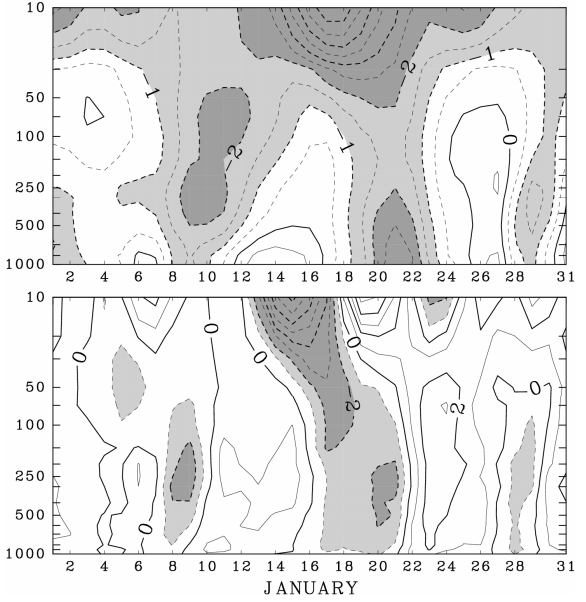


Fig.1. Time-height [pressure (hPa)] cross section of the observed NAM index in January 2003 (upper panel), and the observed zonal-mean zonal wind acceleration (m/s/day) averaged over 50N–70N. Shaded lightly (heavily) are where values are smaller than -1 (-2).

In order to examine the predictability of the SSW by the JMA 1-month ensemble forecast, the time variation of observed and predicted zonal-mean temperature at 80N and 10hPa during January 2003 is

shown in Fig. 2. For the forecasts starting from 1 and 2 January, all the ensemble members failed in predicting the occurrence of the SSW whereas those from 8 and 9 January made successful predictions. Therefore, the SSW event is predictable more than 10 days in advance. This predictable period is somewhat shorter than that of the SSW in December 2001 reported by M05. It should be noted that the spread between the members starting from 15 and 16 January (Fig. 2c) is very small compared with those in Figs. 2a and 2b.

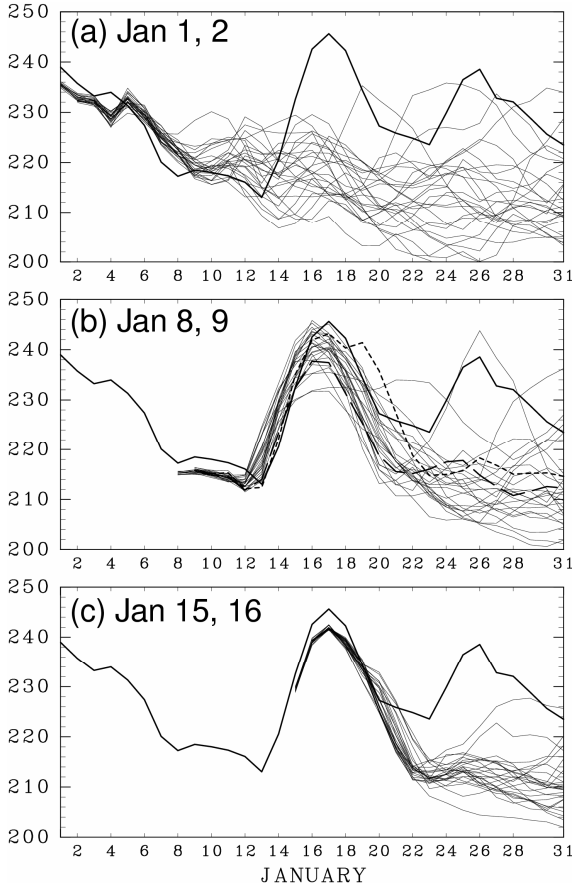


Fig.2. Time variation of the zonal-mean temperature (K) at 80N and 10hPa in January 2003 for the observation (thick solid lines) and the JMA ensemble forecasts (thin solid lines) starting from 1 and 2 January (a), 8 and 9 January (b), and 15 and 16 January 2003 (c). The dotted and broken lines in (b) coincide with run A and run B in Fig. 3, respectively. As regards run A and run B, see the text.

On the other hand, Fig. 3 shows the observed and the predicted NAM index at 1000 hPa (the AO signature). In the following, we will focus on the negative AO event around 21 January just after the SSW. For the forecasts starting from 1 and 2 January, which failed in predicting the SSW, the spread of the

predicted AO signature around 21 January is too large to discuss the predictability of the negative AO event (Fig. 3a). The ensemble members starting from 8 and 9 January, which succeeded in predicting the SSW, also have a large spread for the AO prediction (Fig. 3b). In fact, some members predict a positive AO signature just after the SSW event. Moreover, although all the members starting from one week after (Fig. 3c) predict negative AO signatures around 21 January, the spread of the predicted AO signature is still large. Thus, it is found that the predictable period of the negative AO event is at most 6 days, which is much shorter than that of the precedent SSW event.

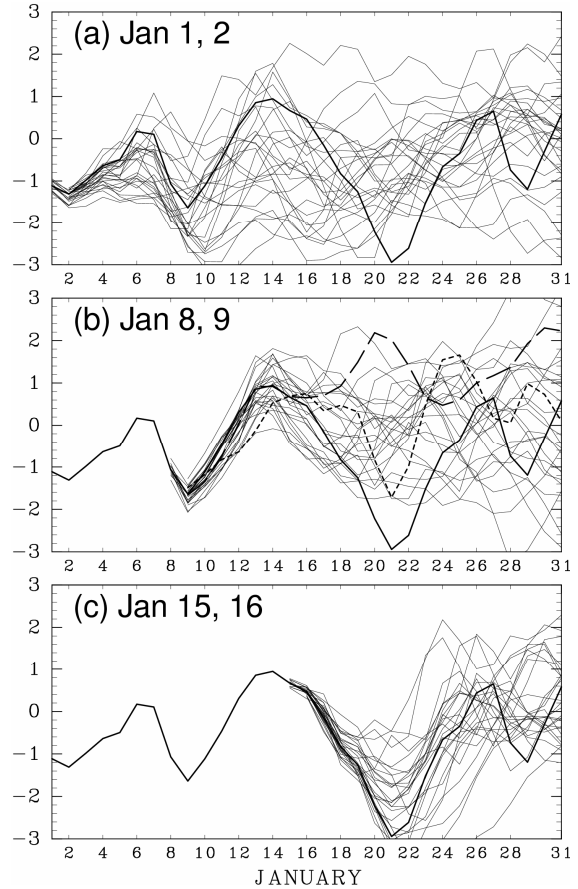


Fig.3. As in Fig. 2, but for AO signature.

In order to reveal the influence of the stratospheric circulation to the prediction of the negative AO event after the SSW, we will examine the ensemble prediction starting from 8 and 9 January in detail (Fig. 3b). At first, we will compare the best (run A; the dotted line) and the worst forecast (run B; the broken line) for the prediction of the negative AO event among the ensemble members. The predicted AO signature by run A (run B) attains the minimum (maximum) value on 21 January among the ensemble members. The

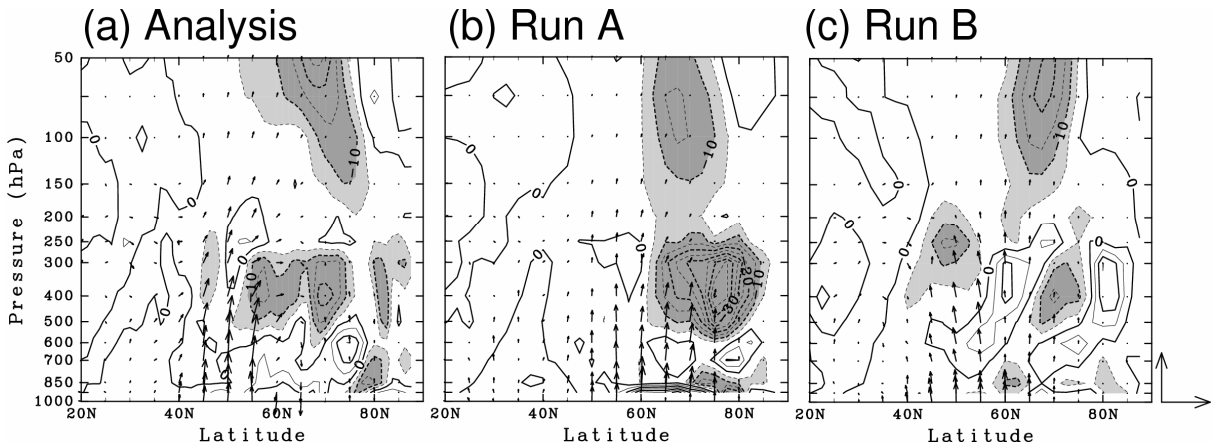


Fig.4. Latitude-height cross sections for the time-mean WN 2 E-P flux (arrows; kg/s^2) and the associated zonal force per unit mass (contours; m/s/day) averaged over 18-20 January 2003. (a) The observation, (b) run A, and (c) run B. Arrows in the right bottom correspond to $(4.0 \times 10^8, 1.5 \times 10^6)$. Shaded lightly (heavily) are where values are smaller than -5 (-10) m/s/day .

analysis based on the transformed Eulerian mean equation reveals that the E-P flux convergence associated with WN 2 components plays a dominant role in the zonal wind deceleration poleward of 50N in the troposphere as well as in the stratosphere after the SSW (not shown).

Then, we investigated the characteristic of WN 2 planetary waves over a 3-day period from 18 to 20 January, when the zonal wind deceleration becomes evident. Figure 4 shows the E-P flux vector and the associated convergence averaged over the 3-day period. For the observation (Fig. 4a), the upward propagation of WN 2 components concentrates around 50N in the troposphere, and there is strong convergence of the E-P flux in the poleward region of the upper troposphere. The wave activity further propagates upward and poleward in the stratosphere, and converges in the middle stratosphere. Run A (Fig. 4b) has a somewhat weaker wave activity than the observation, and the upward propagating region shifts poleward. The convergence of the E-P flux in the upper troposphere is still evident as in the observation. However, for run B (Fig. 4c), the convergence of the E-P flux is considerably weak, and the wave activity tends to propagate equatorward in the upper troposphere, in contradiction to the observation and run A. Therefore, it is necessary to well simulate the behavior of WN 2 planetary waves in the upper troposphere for the prediction of the downward migration of the negative NAM anomaly into the troposphere. Figure 4a also reveals that anomalously enhanced E-P flux

convergence occurs in two discrete regions around the 50-hPa level and the tropopausal region. This suggests that the framework of the gradual downward migration of the negative NAM index from the stratosphere to the lower troposphere is not appropriate for this negative NAM event. Rather, the zonal winds in the troposphere decelerate concurrently with those in the stratosphere.

The propagating property of WN 2 planetary waves during this period is much influenced by the zonal-mean zonal wind distribution during (not shown). In particular, by examining the corresponding refractive index squared for stationary WN 2 component (Andrews et al., 1987), it is found that the slight difference in the zonal-mean zonal wind profile in the tropopausal region around 60N significantly affects the propagating property of the WN 2 component in the upper troposphere. On the contrary, the difference of the refractive index squared in the lower stratosphere is not so evident. The evanescent region with negative refractive index squared prevails in the midlatitudes for the observation and run A as well as run B. The possible relationship between the characteristic zonal-mean zonal wind profile and the subsequent occurrence of the negative AO event is also confirmed by the regression analysis on zonal wind using all ensemble (26) members of the forecast starting from 8 and 9 January as in M05.

1.4 Concluding Remarks

We examined the dynamics and the predictability of a downward migration event of the negative NAM

anomaly occurring in January 2003 just after a SSW by the use of all ensemble members of the 1-month forecasts performed by the JMA. It was found that the E-P flux convergence associated with the WN 2 component plays a dominant role for the downward migration of the negative NAM anomaly while the SSW is caused by the amplification of the WN 1 component. The predictable period of the negative NAM anomaly in the troposphere is 6 days at most, and the ensemble members succeeded in predicting the occurrence of the SSW does not necessarily well predict the following negative NAM anomaly in the troposphere. Thus, the predictability of the negative NAM anomaly in the troposphere is quite limited compared with that of the SSW.

It is also revealed that the fair reproduction of WN 2 planetary waves propagating upward and poleward from the troposphere into the stratosphere is important for the successful prediction of the downward migration of the negative NAM anomaly. The analysis on the refractive index indicates that the tropopausal zonal-mean zonal wind profile rather than the stratospheric zonal-mean zonal wind anomaly after the SSW significantly affects the propagating property of the WN 2 component. Hence, it is suggested that the stratospheric zonal wind anomaly after the SSW can hardly affect the predictability of the tropospheric negative NAM anomaly in comparison with the tropopausal zonal wind anomaly.

Of course, we have to examine other downward migration events of the negative NAM anomaly to confirm our results. Moreover, hindcast experiments using the numerical prediction model is also necessary to reveal the dynamical relationship between the tropopausal zonal wind anomaly and the propagation and the generation of the WN 2 planetary waves during this period.

1.5 Acknowledgments

We would like to thank all the members in Numerical Prediction and Climate Prediction Divisions in JMA for providing us 1-month forecast data sets of JMA. The GFD-DENNOU Library was used for the graphics.

2. Characteristics of damage to buildings and houses caused by strong wind of Typhoon 0613

2.1 Location and Meteorological records

Typhoon 0613 was born on the 10th of September in 2006 and began its approach to Yaeyama Islands on September 15. After passing near by Ishigaki Island, the main island of Yaeyama Islands, it landed by Kyushu, the western to main island of Japan as shown in Fig.5. The maximum peak gust of 67.0m/s has been recorded at 07:19 September 16 at Ishigaki city, which is the second strong wind ever measured at weather station in Ishigaki Island. The typhoon brought a number of strong gusts and tornados during the approach to Kyusyu. There were a strong gust and fore tornados in Miyazaki prefecture, two strong gusts in Oita prefecture and a tornado in Kochi prefecture, which caused damage to buildings and houses. The typhoon also brought strong wind disasters in the Northeast part of Kyusyu as shown in Fig.6.

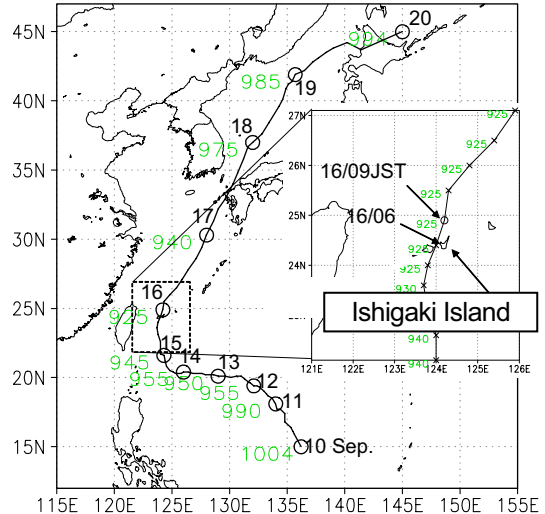


Fig.5 Location of Ishigaki Island and the path of Typhoon 0613.

2.2 Overview of damage

We focus on the strong wind damage in Ishigaki Island and Nobeoka city in this report. The characteristics of damage to buildings and houses were examined.

(1) Ishigaki Island

According to the damage reports later published by the Okinawa Prefectural Government (October, 2006), there were 55 people injured in total, including 4 serious

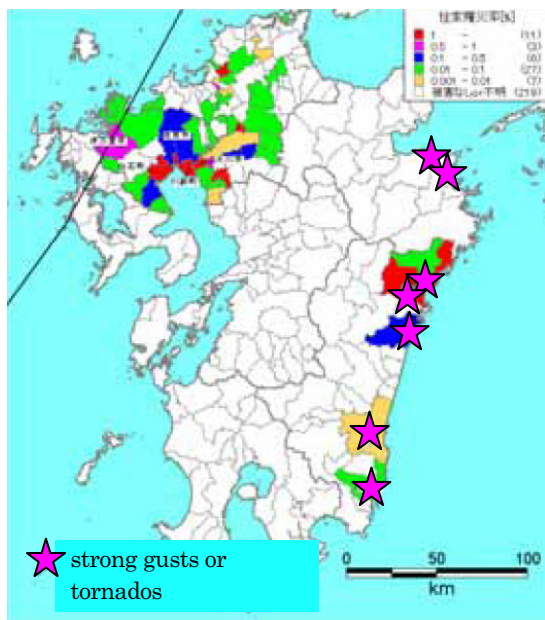


Fig.6 Distribution of damage to buildings and houses in Kyusyu, and locations of strong gusts and tornados.

injuries. A total of 316 buildings and houses were damaged, including 22 houses that were completely destroyed, 50 houses that were badly damaged, 244 houses that were partially damaged. About 4.2 thousand people live in Ishigaki Island with the total number of households at about 2.2 thousand, meaning that 1% of its residents and 14% of its buildings suffered, respectively. The damage was mainly due to strong winds and the cost of damage was estimated to be about 360 million yen (roughly 3 million US\$).

(2) Nobeoka city

According to the damage report published by the Nobeoka city (October, 2006), there were 146 people injured in total, including 3 deaths and 3 serious injuries. A total of 1,180 buildings and houses were damaged, including 79 houses that were completely destroyed, 348 houses that were badly damaged, 753 houses that were partially damaged. About 135 thousand people live in Nobeoka city with the total number of households at about 52 thousand, meaning that 0.1% of its residents and 2.3% of its buildings suffered, respectively. The damage was mainly due to strong winds caused by tornado and the cost of damage was estimated to be about 1.3 million yen (roughly 11 thousand US\$).

2.3 Detail of damage and discussion

Various kinds of damage were caused from the strong winds. Numbers of the damage to roofs, walls and openings has been observed. The roof tiles were blown off (photo 1a). This proceeds to break the roof (photo 1b). Some of less-maintained or old houses were collapsed (photo 1c). Metal roof panels were torn off (photo 2). The ceiling panels under eaves and the walls fell down (photo 3,4). Heavy or huge object such as water tank from the roof was observed (photo 5). Those objects sometimes flew and hit other buildings and houses downwind and damaged to walls or openings (photo 6,7) or cut the electric lines. Every thing might come from collapsed houses in case of very strong winds by tornado (photo 8). The break of opening caused to damage to interior (photo 9,10). The installations indispensable to recovering from the disaster, such as hospital, police office, city office or firehouse and so on, should be highly prevented to the flying missiles. The shutters (photo 11), partitioned sash with small area and thick glass (photo 12) or wind resistant glasses (laminated, tempered, filmed or wired glass) will be effective.

Remarkable damage caused by lightweight houses. Number of steel storehouses or prefabricated houses collapsed (photo 13), got upon the neighboring house (photo 14, 15), blocked the road (photo 16) or broke the telephone poles (photo 17). Usually the lightweight house is simply fastened to the foundations by iron clamps or just set on the ground with small anchors. This can easily blow off (photo 18) or overturn them. Those kinds of disaster could be often occurred in the urban area. Therefore they should be wind resistant designed not to be blown off or be overturned. The damage to telegraph poles is also serious. Cut of electricity is a threat to our daily life. The broken poles block the road and obstruct the traffic and transportation (photo 19).

2.4 Conclusion

This paper reports the results of a survey of strong wind damage caused by Typhoon 0613 in 2006. We examine the characteristics of recent damage to buildings and houses.

To prevent the claddings and openings from the flying missiles is important to reduce the strong wind damage. The shutters and the wind resistant glasses are effective. To decrease the number of missile is also essential. The damage of lightweight houses is notable in urban area.



a. Tearing off of corner roof tiles



b. Damaged roof



c. Collapsed one

Photo 1 Strong wind damage to traditional wooden houses



Photo 2 Torn-off roof tiles
on gymnasium



Photo 3 Fall down of
ceiling panel



Photo 4
Fall down of wall



Photo 5
Fall down of water tank



Photo 6 Damage by missile
of tornado



Photo 7 Hit by
torn-off metal roof



Photo 8 Stack of
flying debris by tornado



Photo 9 Interior damage
by wind and rain



Photo 10 Broken
windows of firehouse



Photo 11 Openings
prevented by shutter



Photo 12 Openings installed



Photo13 Collapsed
partitioned sash with thick glass
storehouse steel construction



Photo14 Lightweight
prefabricated house got
upon the neighbouring house



Photo15 Lightweight steel
storehouse got upon
the neighbouring house



Photo16 Lightweight
prefabricated house
blocked the road



Photo17 Lightweight
prefabricated house
blocked a telegraph pole



Photo18 Remained wooden
foundations of a lightweight
prefabricated house



Photo19 Telegraph poles
blocked the road

3. Gusty Turbulence Structure in the Atmospheric Boundary Layer

2.5 Outline of Observations

Occurrence of disasters by the severe local storms is frequently related to the descending high-speed turbulence in the atmospheric boundary layer.

In order to study the high-speed turbulence structure in the nearly neutral atmospheric boundary layer, observations were carried out at the Shionomisaki Wind Effect Laboratory of Disaster Prevention Research Institute in 1998 and at the Shigaraki MU Observatory of Research Institute for Sustainable Humanosphere, Kyoto University in 2001-2002. For the observation of wind profile in the atmospheric boundary layer, a Doppler sodar was used. From these observations, we selected some cases in which the stability of the boundary layer seems to be nearly neutral.

2.6 Wind Pattern of the High-speed Turbulence Structure

To begin with, we show the typical case observed at Shionomisaki during 1110-1448 LST on 8 Dec. 1998.

In order to detect the high-speed wind events with large-scale structures, we analyze the surface layer turbulence measured by the sonic anemometer (20 m in height) using the integral wavelet transform. In this study, we use the “Mexican hat” wavelet function with a fairly long time scale of 160 s.

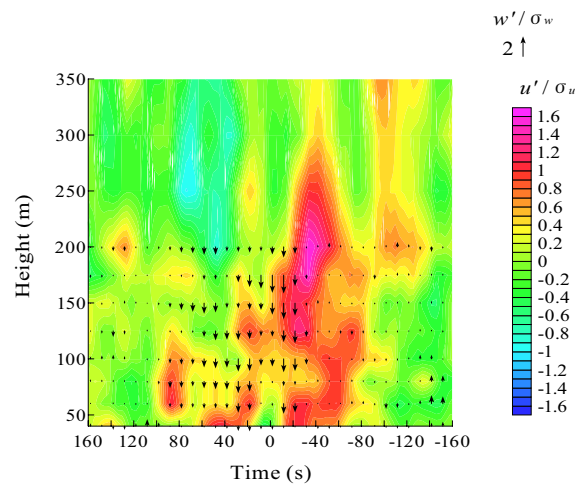


Fig.7 Conditionally averaged wind pattern constructed from the data observed by the Doppler sodar on 8 Dec. 1998 at Shionomisaki

We pick up the high-speed wind events from the local maximum of the wavelet coefficients, which is higher than a threshold value. Then, a conditionally averaged wind pattern on a time-height cross section from detected six events is constructed using the data observed by the Doppler sodar (Fig.7). For the averaging, fluctuating components of the streamwise (u') and vertical (w') velocity components, which are normalized using their variances, are used. In the figure, the contours depict the normalized u' values and the arrows show the normalized w' values.

This figure shows a descending high-speed turbulence structure, the central part (maximum u' value) of which is located at the height near 200 m and at the time near 30 s before the time of the detected events. Before the high-speed structure, a low-speed turbulence structure, which is slightly ascending at the time near 140 s before the event time, is also represented.

This pattern is similar to the previously presented structures by the observation (Gao et al., 1989). They showed the microfrontal structures for the scalar concentration and the ejection-sweep structures for the velocities. In our case, structures could be investigated over a wide range of height using the Doppler sodar.

Similar wind patterns, which show high-speed turbulence structures, are depicted in other observation cases. Therefore, it is certain that turbulence structure depicted in Fig. N1 appears commonly in the nearly neutral atmospheric boundary layer.

2.7 Research on the Environmental Condition Concerning to a Tornadic Outbreak in Hokkaido

On November 7 at about 13:20 a severe tornado (Tatsumaki) hit Saroma, Hokkaido. In this tornado outbreak, 47 houses (including residential houses and non-residential houses) were completely destroyed and 57 were half or partly destroyed. What is worse were 9 persons were killed and 26 persons were injured. The photo 20 shows a major damaged area in Saroma town.

It is known that development of severe storm and the associated tornado outbreaks in the United States relate on the atmospheric static stability and the vertical wind sheer. Typical parameters used in the assessment of tornado risk are Energy Helicity Index (EHI) expressed as

$$EHI = \frac{CAPE \times SREH}{1.6 \times 10^5}$$



Photo 20 Damage of town caused by the tornado (Photo is taken by Shin Corp.)

The EHI is the multiple of *CAPE* (Convective Available Potential Energy),

$$CAPE = g \int_{LFC}^{ZE} \frac{\theta(z) - \bar{\theta}(z)}{\bar{\theta}(z)} dz$$

and *SREH* is the Storm Relative Environmental Helicity,

$$SREH = - \int_{0km}^{3km} \mathbf{k} \cdot \left[(\mathbf{V}(z) - \mathbf{c}) \times \frac{\partial \mathbf{V}(z)}{\partial z} \right] dz.$$

The *CAPE* represents the environmental potential for the development of deep convection and the *SREH* represents the potential for vortex generation. When and where both *CAPE* and *SRRH* have high value, severe storm accompanying tornado is favorable to occur. The typical values of these parameters for the tornado outbreak in United States are shown in Table 1 according to Bluestein and Jain (1985) and Rasmussen and Blanchard (1998).

If the EHI is to be used as an indicator of tornado outbreak even in Japan, there will be possibility to predict tornado outbreaks in Japan. Thus, values of these parameters are computed using the Grid Point Value data of operational numerical prediction conducted by Japan Meteorological Agency.

The JMA_MSM runs 8 times a day initialized at 00, 03, 06, 09, 12, 15, 18 and 21JST. In this study 4 run initialized at 03, 06, 09, 12JST on Nov. 7 are used. Using the 3-hourly output of prediction the distribution of *EHI* is computed for 12 and 15 JST as shown in Fig.8. In the figure, for example, the left-top panel shows the *EHI* at 12 JST computed from prediction initialized at 03JST and the right-bottom panel shows that at 15JST initialized at 12JST. In the figure places of Saroma Town and other wind hazard are also shown.

It is seen that the *EHI* computed from the prediction

initialized at 09JST well covers major wind hazards, tornado at Hidaka-cho, High wind at Rikubetsu-cho and tornado at Saroma-cho. In 12JST distribution, a high EHI area is seen near Hidaka-cho, and at 15JST a band of high value (*EHI*>0.2) extend from south which covers Saroma-cho. The Value is 0.55 near Saroma-cho, which is comparable to the EHI value for weak tornadoes in United States in Table 1. The predictions initialized at 03 and 06 JST yield higher value of *EHI* but the distribution is very wide, so that it is difficult to judge the local potential for tornado outbreak from these results.

Although *EHI* distribution from prediction initialized at 09JST shows good agreement with tornado outbreaks, other high *EHI* areas are found near Kushiro and Shiretoko areas where no wind hazards took place. Further, it seems that the *EHI* value seem to increase generally with the increase of prediction time. Before using *EHI* as an indicator of potential for tornado outbreaks, further studies are necessary. One of difficulties for this study is that the number of tornado outbreak is rather small to perform statistical evaluation for the performance of *EHI*. We have to collect tornado cases as many as possible.

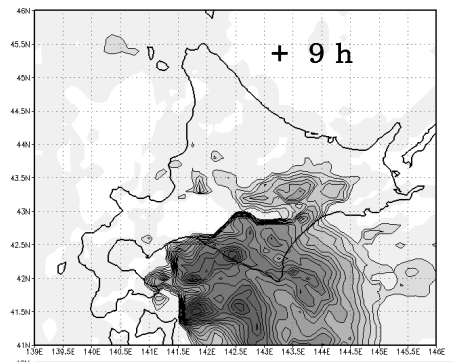
Table 1 The median of CAPE, SREH and EHI for investigated cases of tornado outbreak in United State

	F2≤ tornadoes	F0 and F1 tornadoes
<i>CAPE</i>	1314	1152
<i>SREH</i>	180	124
<i>EHI</i>	1.48	0.64

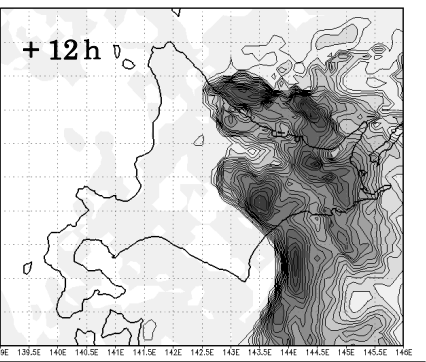
Initial

EHI at 12JST

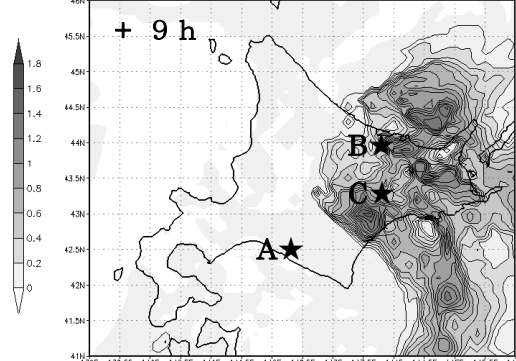
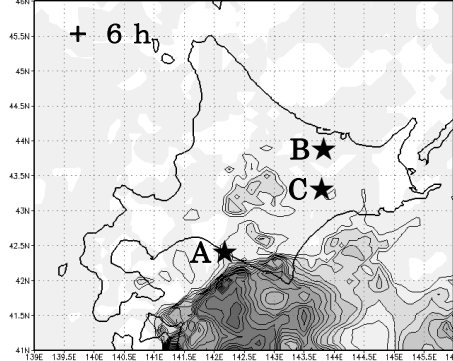
03JST



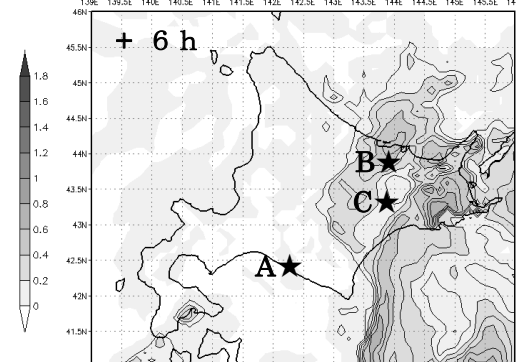
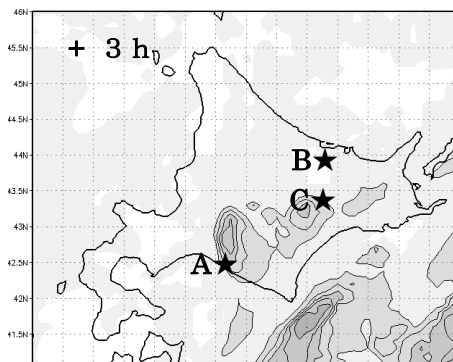
EHI at 15JST



06JST



09JST



12JST

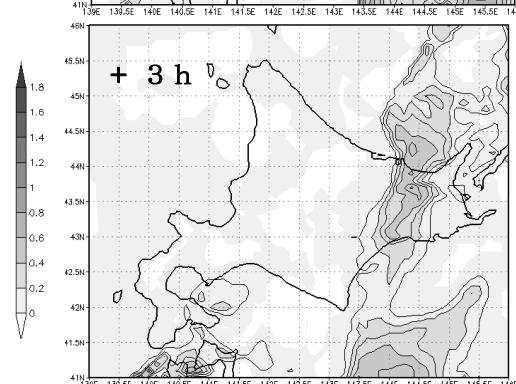
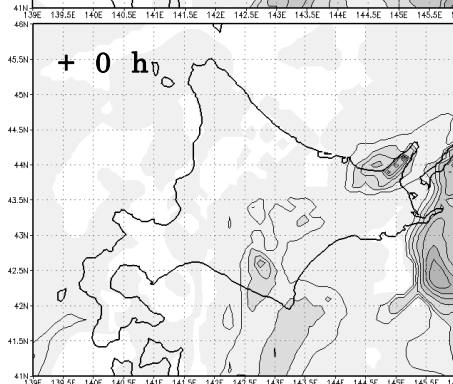


Fig.8 The distribution of EHI at 12JST and 15 JST computed MSM prediction initialized at 03, 06, 09 and 12JST. The A, B and C in the figures denote the places of tornado at Hidaka-cho (11:40), tornado at Saroma-cho (13:20)、and wind gust at Rikubetu/Asyoro area (14:30).

References

- Andrews, D.G., Holton, J.R. and Leovy, C.B. (1987): Middle Atmosphere Dynamics. Academic Press, pp. 489.
- Baldwin, M.P. and Dunkerton, T.J. (1999): Propagation of the Arctic Oscillation from the stratosphere to the troposphere. *J. Geophys. Res.*, Vol. 104, pp.30937-30946.
- Baldwin, M.P. and Dunkerton, T.J. (2001): Stratospheric harbingers of anomalous weather regimes. *Science*, Vol. 294, pp.581-584.
- Baldwin, M.P., Stephenson, D.B., Thompson, D.W.J., Dunkerton, T.J., Charlton, A.J. and O'Neil, A. (2003): Stratospheric memory and skill of extended-range weather forecasts. *Science*, Vol. 301, pp.636-640.
- Blackmon, M. L., (1976): A climatological spectral study of the 500mb geopotential height of the Northern Hemisphere. *J. Atmos. Sci.*, Vol. 33, pp.1607-1623.
- Mukougawa, H. and Hirooka, T. (2004): Predictability of stratospheric sudden warming: A case study for 1998/99 winter. *Mon. Wea. Rev.*, Vol. 132, pp.1764-1776.
- Mukougawa, H., Sakai, H. and Hirooka, T. (2005): High sensitivity to the initial condition for the prediction of stratospheric sudden warming. *Geophys. Res. Lett.* Vol. 32, L17806, doi:10.1029/2005GL022909.
- Toth, Z. and Kalnay, E. (1993): Ensemble forecasting at NMC: The generation of perturbations. *Bull. Am. Met. Soc.*, Vol. 74, pp.2317-2330.
- Yamazaki, K. and Shinya, Y. (1999): Analysis of the Arctic Oscillation simulated by AGCM. *J. Meteor. Soc. Japan*, Vol. 77, pp.1287-1298.
- Yasunari, T., 1979: Cloudiness fluctuations associated with the Northern Hemisphere monsoon. *J. Meteor. Soc. Japan*, 58, 225-229.
- Disaster Report of tornado on September 17 in Heisei 18, Nobeoka city, (October, 2006).
- Disaster Report (prompt version) of Typhoon 13 in Heisei 18, Okinawa Prefectural Government, (October , 2006).
- Gao, W., Shaw, R.H. and Paw U, K.T. (1989): Observation of organized structure in turbulent flow within and above a forest canopy, *Boundary-Layer Meteorol.*, Vol. 47, pp.349-377.
- Bluestein, H. B. and M. H. Jain: Formation of mesoscale lines of precipitation: Severe aquall line in Oklahoma during the spring, *J. Atmos. Sci.*, 42, 1711-1732, 1985.
- Rasmussen E. N. and D. O. Blanchard: A baseline climatology of sounding-derived super cell and tornado forecast parameters, *Weather Forecasting*, 13, 1148-1164, 1998

異常気象とそれに伴う災害の実態把握と予測に関する研究

河井宏允・岩嶋樹也・石川裕彦・丸山敬・向川均
堀口光章・井口敬雄・荒木時彦

要旨

本報告は、異常気象を引き起こす原因の解明と、それによってもたらされる災害の実態について述べたもので3章からなっている。第1章は2003年1月の成層圏突然昇温(SSW)に引き続いで生じた北半球環状モード(NAM)負偏差の下方伝播の予測可能性について、気象庁一ヶ月予報結果を用いて解析を行った結果を示したものである。解析の結果、このNAM負偏差の予測可能な期間はせいぜい6日程度であり、NAM偏差の予測には対流圏界面付近における波数2の惑星規模波を正しく再現しなければならないことが明らかとなった。第2章は、2006年に起った台風、竜巻及び突風による建物強風被害の調査結果について示した。台風0613号では八重山諸島や九州で建物が大きな強風被害を受けたうえ、この台風に伴って多くの竜巻や突風が発生した。延岡市では3名が竜巻によって死亡、JR日豊本線の特急“にちりん”が脱線した。また、11月7日には北海道佐呂間町で竜巻が発生、9名もの死者を出した。第2章では、これらの強風による建物被害の特徴を検証し、防災・減災の観点から有効な対策を考えた。第3章では、ほぼ中立な安定度の大気境界層中における下降する強風の乱流構造について、観測によりその風速分布の様子を明らかにするとともに、北海道佐呂間町で発生した竜巻に関して、環境パラメーターから発生予測を行う可能性を検討した。

キーワード:予測可能性、アンサンブル予報、成層圏突然昇温、台風0613号、竜巻、突風、建物被害、乱流構造、大気境界層、EHI